J Solid State Electrochem (2007) 11:1365–1373
DOI 10.1007/s10008-007-0294-4

ORIGINAL PAPER

Changes in surface stress of gold electrode during underpotential deposition of copper

Masahiro Seo · Makiko Yamazaki

Received: 16 January 2007 / Revised: 13 February 2007 / Accepted: 16 February 2007 / Published online: 6 March 2007

Abstract The changes in surface stress of the evaporated gold electrode (mainly oriented to the (111) plane) during underpotential deposition (UPD) of copper in 0.1 M sulfuric acid medium or 0.1 M perchloric acid medium with and without sulfate or chloride were measured using a bending beam method. The surface stress maximum of gold electrode appeared during Cu-UPD. The co-adsorption of (bi)sulfate or chloride ions with copper atoms induced the compressive surface stress to promote the Cu-UPD. The factors influencing the surface stress or surface elastic strain were discussed in relation to the Cu-UPD structure.

Keywords Surface stress · Underpotential deposition of copper · Gold electrode · Co-adsorption of anions · Bending beam method

Introduction

Underpotential deposition (UPD) of foreign metal atoms on a noble metal electrode is one of the most interesting subjects from the viewpoint of surface energetics, as the structural changes of an adlayer for many UPD systems [1] take place spontaneously towards the more energetically stable direction. In a solid metal electrode subjected to an elastic deformation, the surface stress g or surface elastic strain ε is an important parameter of surface energetics. The other surface energetic parameter is the surface tension γ for a liquid metal electrode such as mercury subjected to a plastic deformation.

In the case where a solid metal electrode is isotropic, g and ε become scalar, and the following Shuttleworth equation [2] holds between two surface energetic parameters, g and γ.

$$g = \gamma + \partial\gamma/\partial\varepsilon \tag{1}$$

Moreover, the Gibbs adsorption isotherm for an isotropic solid electrode is given by

$$d\gamma = -q_m dE - \sum_i \Gamma_i d\mu_i + (g-\gamma)d\varepsilon, \tag{2}$$

where q_m is the surface charge density of the electrode; E the electrode potential; Γ_i the surface excess of ith species; and μ_i the chemical potential of ith species. Lipkowski et al. [3] have shown that the term $(g-\gamma)\, d\varepsilon/dE$ is negligibly small. Láng and Heusler [4, 5] and Gutman [6], however, claimed that the validity of Eq. 2 was questioned because of a mathematical incorrectness in its derivation. Seo et al. [7, 8] found from the measurement of changes in surface stress that the difference between $\partial g/\partial E$ and $\partial\gamma/\partial E$ is significantly large in the cases where iodide ions are adsorbed on gold and hydroxide ions are adsorbed on platinum, accompanying a charge transfer. Friesen et al. [9] measured the changes in surface stress for the UPD systems such as Pb^{2+}/Au(111) and emphasized that the changes in surface stress include the differences in intrinsic surface stress and in interface stress between adlayer and substrate and the coherency surface stress. Friesen et al. [9] eventually determined the compressive interface stress for the incommensurate Pb/Au (111) interface to be 1.76 J m^{-2} from the surface X-ray scattering (SXS) results of Pb-UPD layer by

Dedicated to Professor Su-Il Pyun on the occasion of his 65th birthday.

M. Seo (✉) · M. Yamazaki
Graduate School of Engineering, Hokkaido University,
Kita-13 Jo, Nishi-8 Chome,
Kita-ku, Sapporo 060-8628, Japan
e-mail: seo@elechem1-mc.eng.hokudai.ac.jp

Toney et al. [10]. The value of the compressive interface stress for the incommensurate Pb/Au(111) interface was consistent with that obtained from the measurement of changes in surface stress by Seo et al. [11].

Shi et al. [12–16] obtained thermodynamically the surface excess of each component from the chronocoulometrical studies of Au(111) electrode during Cu-UPD in perchlorate solutions containing Cu^{2+} and SO_4^{2-} or Cl^- and indicated that the co-adsorption of Cu atoms and SO_4^{2-} or Cl^- proceeds on Au (111) electrode surface. Moreover, scanning tunneling microscopy (STM) [17–19], SXS [20], and surface extended X-ray absorption fine structure (SEXAFS) [21–23] studies showed that the Cu-UPD structures on Au (111) were different in the presence of SO_4^{2-} and Cl^-. Trimble et al. [24] have recently claimed that the driving force for the reconstruction of fcc (111) metal surfaces is associated with the difference between g and γ, i.e., the quantity of $(g-\gamma)$ which involves the term of surface elastic strain as seen from Eq. 2.

The surface strain induced by co-adsorption of electrolyte anions would influence the Cu-UPD structure on Au (111) electrode. The measurement of surface tension by chronocoulometry is unable to provide any information of surface strain. In contrast, the information of surface strain may be obtained from the measurement of surface stress. In this study, the changes in surface stress of Au (111) electrode during Cu-UPD process were measured by using a bending beam method to understand the role of surface strain in UPD structure depending on co-adsorption of SO_4^{2-} and Cl^-.

Experimental

Bending beam method

The changes in surface stress Δg for a thin metal film on one side of a glass plate in contact with the solution were measured from the changes in curvature of the plate. If the thickness of the film t_f is sufficiently less than the thickness of the plate t_s, Δg can be obtained by using Stoney's equation [25]

$$\Delta g = \left[E_s t_s^2/6(1-\upsilon_s)\right]\Delta(1/R), \tag{3}$$

where E_s, ν_s, and R are the Young's modulus, the Poisson's ratio, and the curvature radius of the plate, respectively. In derivation of Eq. 3, it is assumed that $\Delta g = t_f \Delta\sigma_f$ where $\Delta\sigma_f$ is the change of the film stress. The values of $\Delta(1/R)$ can be calculated from the changes $\Delta\theta$ of the deflection angle θ of a laser beam mirrored by the metal layer on the plate. If a laser beam is irradiated perpendicular to the plate with a thin metal layer which is placed vertically into an electrochemical cell with an optical window, the following approximate equation can be derived for large R and L and small θ.

$$\Delta(1/R) \approx \Delta\theta/2L, \tag{4}$$

where L is the distance between the solution level in the cell and the reflection point of the laser beam on the glass plate. The set-up of the bending beam method used in this study is shown in Fig. 1 [7, 26–28]. The reflected laser beam is directed toward a position-sensitive photodetector (PSD) located at a distance of W from the glass plate. The changes Δa in position of the reflected beam on PSD due to bending of the glass plate can be calibrated from the changes in dc output signals of the PSD. Moreover, the approximate relation between $\Delta\theta$ and Δa can be derived from the geometry shown in Fig. 1.

$$\Delta\theta \approx \Delta a/n_s W, \tag{5}$$

where n_s is the refractive index of the solution. As the laser beam is reflected inside the solution and the deflection is measured in air outside the cell, n_s has to be taken into consideration [26, 29]. Consequently, the following relation can be obtained with good approximation from Eqs. 3, 4, and 5.

$$\Delta g \approx \left[E_s t_s^2/6(1-\nu_s)\right](\Delta a/2n_S LW). \tag{6}$$

As the actual values of E_s, t_s, ν_s, n_s, L, and W are known, Δg can be calculated by determining experimentally Δa.

Preparation of working electrode and electrolytes

The working electrode was prepared by evaporating a 220 nm thick gold layer on a very thin titanium layer evaporated onto one side of a glass plate (thickness t_s= 150 μm; width w_s=5.0 mm; total length l_s=60 mm; Young's modulus E_s=70.9 GPa; Poisson's ratio ν_s=0.23). It was confirmed by a thin film X-ray diffraction that the evaporated gold layer was mainly oriented to the (111) plane. The electrolytes used in this experiment were the following solutions: (a) 0.1 M H_2SO_4, (b) 0.1 M H_2SO_4+10^{-3} M $CuSO_4$, (c) 0.1 M $HClO_4$+10^{-3} M $Cu(ClO_4)_2$+10^{-3} M KC lO$_4$, (d) 0.1 M $HClO_4$+10^{-3} M $Cu(ClO_4)_2$+10^{-3} M K_2 SO_4, and (e) 0.1 M $HClO_4$+10^{-3} M $Cu(ClO_4)_2$+10^{-3} M KCl. The electrolytes (a) and (b) were chosen, as the Cu-UPD structures on Au(111) in sulfuric acid media were well investigated by STM, SXS and etc., whereas the electrolytes (c), (d), and (e) were chosen to investigate the effects of co-adsorbed anions on surface stress or surface strain associated with Cu-UPD structures. These electrolytes were prepared from guaranteed reagent grade chemicals with ultrapure water supplied through a super Millipore Milli Q filter system. Before introduction to the electrochemical cell, the electrolytes were deaerated with ultrapure argon gas in solution reservoirs.

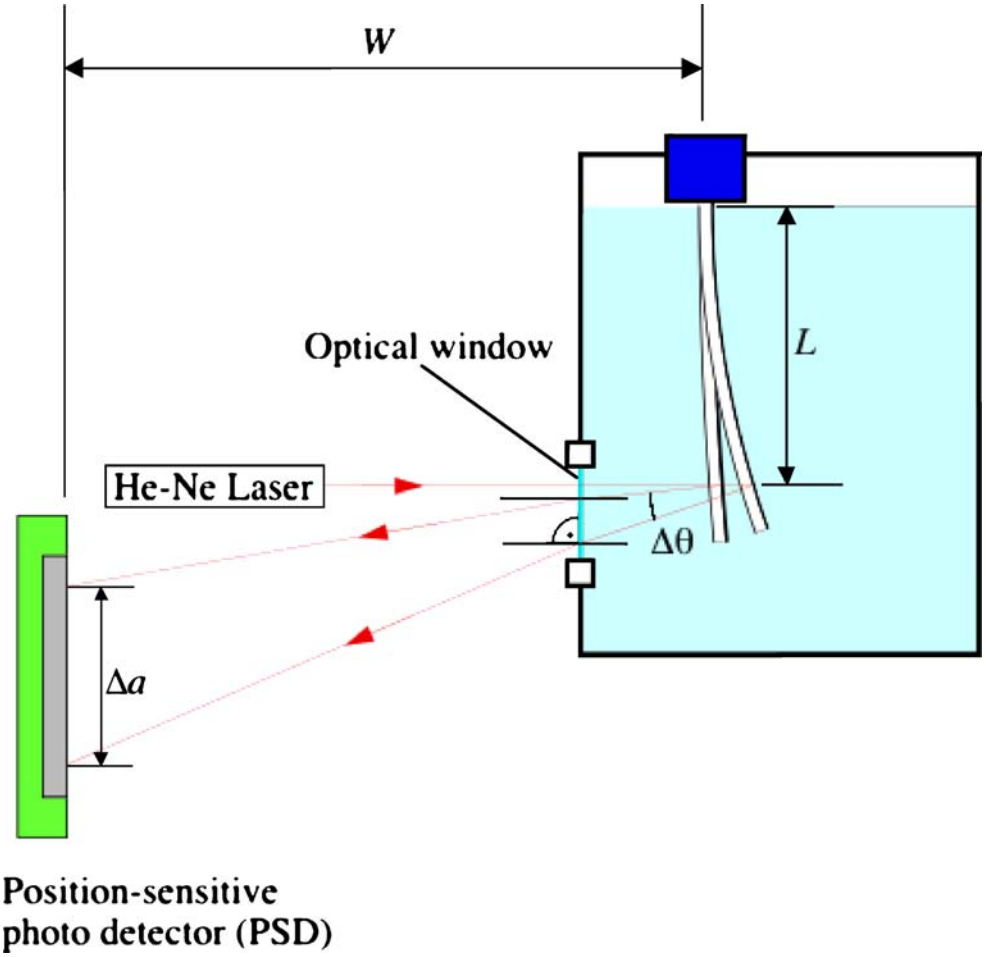

Fig. 1 Scheme of the bending beam set-up. $\Delta\theta$ change in the deflection angle θ of the He–Ne laser beam mirrored by the metal layer on the plate; L distance between the solution level in the cell and the reflection point of the laser beam on the glass plate; W distance between the glass plate and the position sensitive photo detector (PSD); Δa change in position of the reflected beam on PSD due to bending of the glass plate

Measurements of cyclic voltammogram and changes in surface stress

A gold plate was used as the counter electrode. The electrode potential was measured with an Ag/AgCl electrode in a saturated KCl solution and converted to the standard hydrogen electrode (SHE) scale. The cyclic voltammogram (CV) was measured at a potential sweep rate of 5 mV s^{-1} in the potential range between 0.80 and 0.25 V (SHE). The anodic potential limit was chosen at 0.8 V (SHE) to avoid the onset of the surface oxygenation reaction on gold, whereas the cathodic potential limit was chosen at 0.25 V (SHE), corresponding to the equilibrium potential of Cu/Cu^{2+} (10^{-3} M).

For measurement of the changes in surface stress, He–Ne laser was used, and PSD (Hamamatsu S1300) was located at a distance of W=60 cm from the working electrode. The distance between the solution level in the cell and reflection point of the laser beam on the glass plate was L=40 mm. The changes in current and *dc* output signals of the PSD were measured simultaneously as a function of electrode potential or time and recorded on a personal computer. The temperature of solution in the cell was kept at 25 °C. The same value of refractive index n_s=1.34 was used for all the electrolytes used in this experiment, as the value of n_s for 0.1 M electrolyte did not depend on its composition (perchloric acid or sulfuric acid).

Results and discussion

Changes in surface stress during Cu-UPD in sulfuric acid medium

Figure 2 shows the CVs and surface stress Δg vs electrode potential E curves in the electrolytes (a) dotted line and (b) solid line. The CV in the electrolyte b has the typical cathodic (A_1 and A_2) and anodic (D_1 and D_2) peaks, the potential positions of which are consistent with those observed so far for the Cu-UPD on Au (111) electrode in sulfuric acid media [18, 30]. Two pairs of peaks (A_1/D_1 and A_2/D_2) are associated with two different adsorption and desorption processes of Cu atoms. For the Δg vs E curves in the electrolytes (a) and (b), it is noted that the standard point of Δg=0 was taken at 0.80 V (SHE), as the adsorption of Cu atoms would not proceed at 0.80 V (SHE) in the

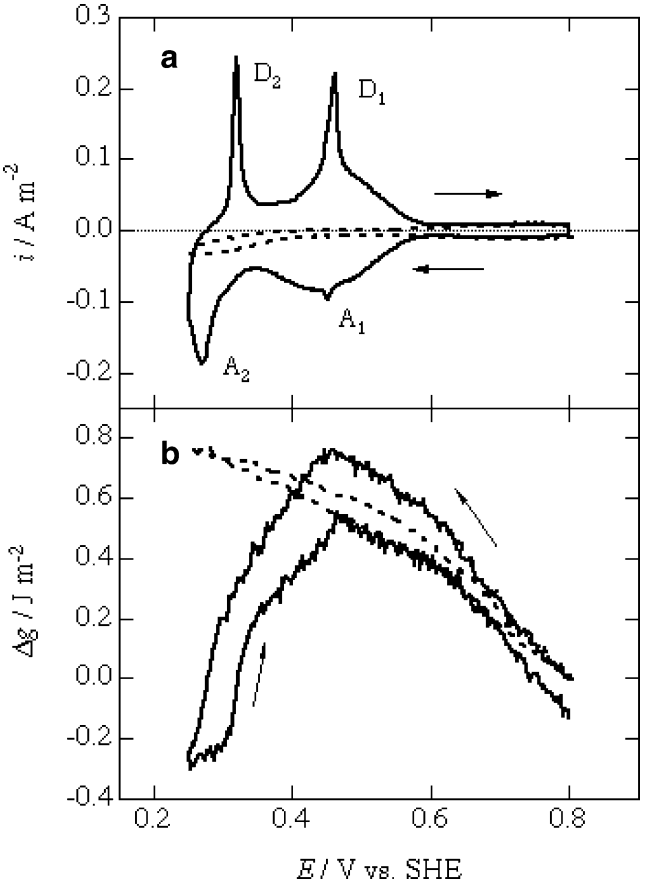

Fig. 2 **a** Cyclic voltammograms and **b** Δg vs E curves obtained at a potential sweep rate of 5 mV s^{-1} in the potential range between 0.80 and 0.25 V (SHE) for the evaporated gold electrode (mainly oriented to the (111) plane) in the electrolytes (a) 0.1 M H_2SO_4 (*dotted line*) and (b) 0.1 M H_2SO_4+10^{-3} M $CuSO_4$ (*solid line*)

electrolyte (b), whereas the adsorption of SO_4^{2-} would proceed to the same extent in both electrolytes (a) and (b). It is also noted that the increase and decrease in Δg mean the changes in surface stress to the tensile and compressive directions, respectively. The Δg vs E curve in the electrolyte, although some hysteresis is present, has the maxima of Δg at 0.44 V (SHE) in the cathodic potential sweep and at 0.47 V (SHE) in the anodic potential sweep, which correspond to the A_1 cathodic and D_1 anodic peaks, respectively, in the CV. Moreover, the Δg vs E curve has the bending points at 0.28 V (SHE) in the cathodic potential sweep and at 0.33 V (SHE) in the anodic potential sweep, which correspond to the A_2 cathodic and D_2 anodic peaks, respectively, in the CV.

In contrast, the Δg vs E curve in the electrolyte (a) has no maxima of Δg and no bending points, that is, Δg increases and decreases monotonously with cathodic and anodic potential sweeps, respectively. It is seen from comparison of the CVs between electrolytes (a) and (b) that the Cu-UPD starts at 0.60 V (SHE) in the cathodic potential sweep. The surface stress still changes to the tensile direction, i.e., $\Delta(\Delta g)>0$ during cathodic potential sweep from 0.60 to 0.44 V (SHE) where the Cu-UPD proceeds. In spite of that, the Cu-UPD proceeds in the potential region between 0.60 and 0.44 V, the atomic force microscopy (AFM) image lacked in atomic resolution [18], indicating that the Cu adatoms are mobile and randomly deposited on the electrode surface together with some (bi) sulfate anions [1]. After the A_1 peak in the cathodic potential sweep, the surface stress changes to the compressive direction, i.e., $\Delta(\Delta g)<0$. The STM images [18, 30, 31] showed that the Cu-UPD layer formed at 0.40 V (SHE) in the potential region between A_1 and A_2 peaks has a honeycomb $\left(\sqrt{3}\times\sqrt{3}\right)R30^\circ$ structure with (bi) sulfate ions occupying the centers of the honeycomb, which was confirmed by SXS [20] and SEXAFS [32] and was also supported by electrochemical quartz crystal microbalance [33, 34]. The slope of the Δg vs E curve in the electrolyte (b) rises sharply to the compressive direction after the A_2 peak in the cathodic potential sweep. The STM [31] and AFM [35, 36] images showed that the Cu-UPD layer formed on Au (111) after the A_2 peak had a Cu-(1×1) commensurate structure. Moreover, the SEXAFS [21, 22] revealed that (bi) sulfate ions are adsorbed on top of the Cu-(1×1) monolayer. The cathodic charge density Δq_c calculated between 0.60 and 0.25 V (SHE) in the cathodic potential sweep from the CV for the electrolyte (b) is about 4.9 C m^{-2}, which is close to 4.4 C m^{-2} [1] necessary for the deposition of a fully discharged monolayer of copper if the surface roughness of Au electrode r=1.1 is taken into account.

As seen from Fig. 2, the difference in Δg between electrolytes (b) and (a) is −1.1 J m^{-2} at the cathodic potential limit of 0.25 V (SHE) corresponding to the formation of Cu-(1×1) monolayer. Trimble et al. [37], using a bending beam method, measured the changes in surface stress of Au (111) electrode in acidic sodium sulfate (pH 2) electrolytes with and without 10^{-3} M Cu^{2+}, and they reported that the difference in Δg between the electrolytes with and without Cu^{2+} was −0.6 J m^{-2} at the potential corresponding to the formation of Cu-(1×1) monolayer, which is about 0.5 times as much as that (−1.1 J m^{-2}) obtained by the present study. On the other hand, according to the Δg vs E curves measured by Kongstein et al. [38] for the Au (111) electrode in 0.1 M sulfuric acid solutions with and without 10^{-2} M Cu^{2+}, the difference in Δg between the electrolytes with and without Cu^{2+} is about −1.0 J m^{-2} at the potential corresponding to the formation of Cu-(1×1) monolayer, which is close to that obtained by the present study. These discrepancies between the Δg vs E curves measured by Trimble et al. [37], Kongstein et al. [38], and ours may result from the differences in preparation of working electrode, solution pH, cation species in solution, potential sweep rate, and anodic potential limit, although the reasons are not clear.

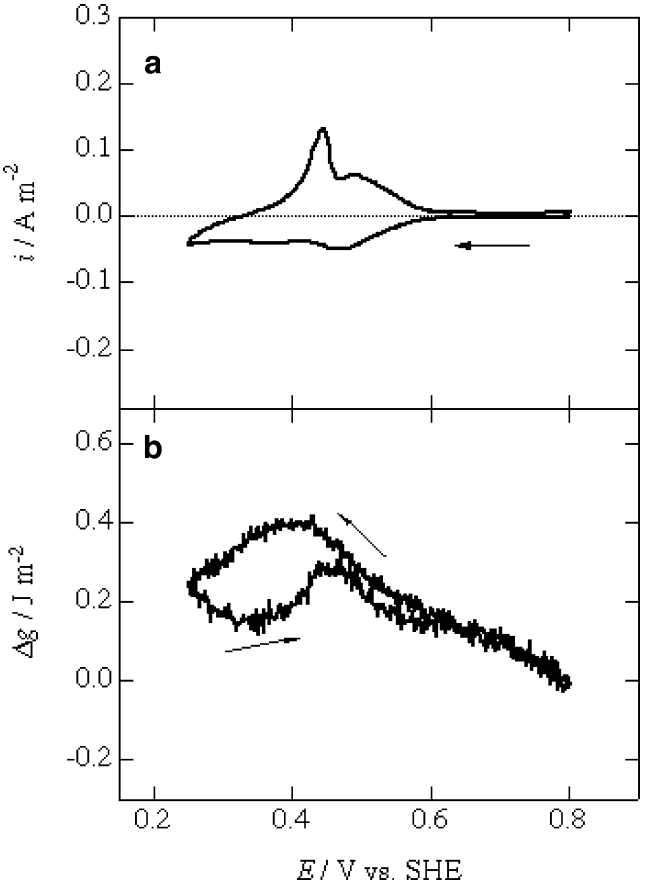

Fig. 3 **a** Cyclic voltammogram and **b** Δg vs E curve obtained at a potential sweep rate of 5 mV s^{-1} in the potential range between 0.80 and 0.25 V (SHE) for the evaporated gold electrode (mainly oriented to the (111) plane) in the electrolyte (c) 0.1 M $HClO_4$+10^{-3} M $Cu(ClO_4)_2$+10^{-3} M $KClO_4$

Changes in surface stress during Cu-UPD in perchloric acid medium containing sulfate or chloride

Figures 3, 4, and 5 show the CVs and Δg vs E curves in the electrolytes (c), (d), and (e), respectively. The cathodic charge density Δq_c calculated between 0.60 and 0.25 V (SHE) in the cathodic potential sweep from the CV of Fig. 3 is about 2.4 C m^{-2}, which is only less than 50% of those calculated from the CVs of Figs. 4 and 5, indicating that Cu-UPD does not proceed sufficiently up to the cathodic potential limit of 0.25 V (SHE) in perchloric acid medium without sulfate or chloride. The shape of the CV in Fig. 3 is similar to that of the CV obtained for the Cu-UPD on Au (111) in 0.1 M $HClO_4$+10^{-2} M $Cu(ClO_4)_2$ solution by Hotlos et al. [19] who indicated that the broad cathodic and anodic peaks in the CV are associated with trace amounts of Cl^- ions (ca. 10^{-6} M) contained in the electrolyte as impurity. This means that perchlorate ions suppress the Cu-UPD on Au (111). The cathodic and anodic current peaks in the CV (Fig. 4) for the electrolyte (d) are not sharp as compared with those in the CV (Fig. 2) for the electrolyte (b), which may be caused by the presence of a large majority of perchlorate ions in the electrolyte (d). The Δg vs E curves, as well as the CVs, reflect sensitively the difference in Cu-UPD process between electrolytes (c), (d), and (e). For the electrolyte (c), the maxima of Δg are observed at 0.40 V (SHE) in the cathodic potential sweep and at 0.45 V (SHE) in the anodic potential sweep. The change in Δg from 0.40 to 0.25 V (SHE) in the cathodic potential sweep is $\Delta(\Delta g)$=−0.17 J m^{-2}. The STM images [19] of Au (111) in 0.1 M $HClO_4$+ 0.01 M $Cu(ClO_4)_2$ containing small amounts of Cl^- ions ($\leqq 10^{-6}$ M)showed a "(5×5)" structure in the potential range between 0.60 and 0.40 V (SHE) and a (2×2) superstructure at potentials negative of 0.40 V (SHE). Careful measurements [19] indicated that the "(5×5)" structure is not a real (5×5), but an incommensurate, structure between (4×4) and (5×5).

For the electrolyte (d), the maxima of Δg emerge at 0.45 V (SHE) in the cathodic potential sweep and at 0.46 V (SHE) in the anodic potential sweep. The change in Δg from 0.45 to 0.25 V (SHE) in the cathodic potential sweep is $\Delta(\Delta g)$=−0.80 J m^{-2}. Shi and Lipkowski [12, 13], using

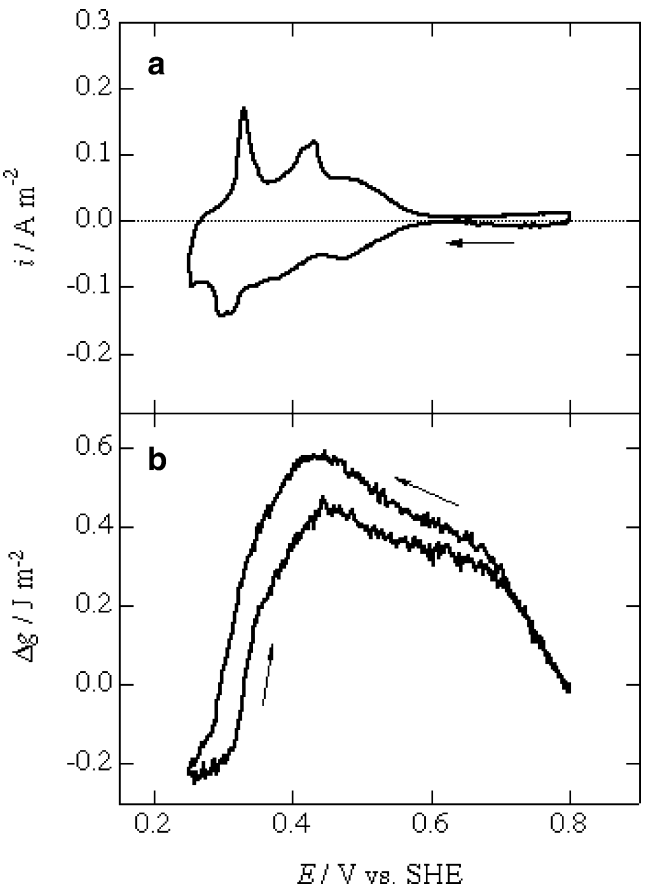

Fig. 4 **a** Cyclic voltammogram and **b** Δg vs E curve obtained at a potential sweep rate of 5 mV s^{-1} in the potential range between 0.80 and 0.25 V (SHE) for the evaporated gold electrode (mainly oriented to the (111) plane) in the electrolyte (d) 0.1 M $HClO_4$+10^{-3} M $Cu(ClO_4)_2$+10^{-3} M K_2SO_4

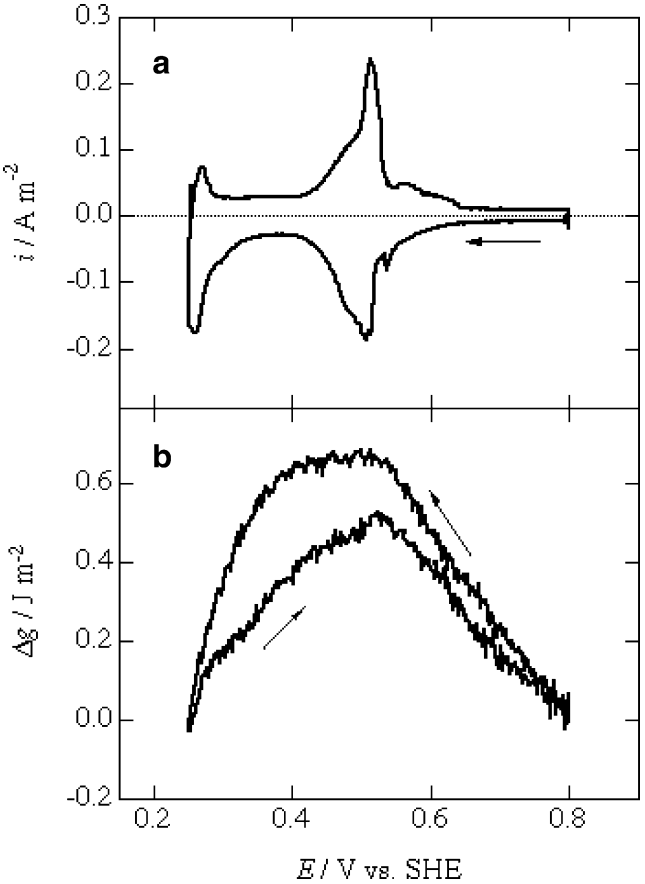

Fig. 5 **a** Cyclic voltammogram and **b** Δg vs E curve obtained at a potential sweep rate of 5 mV s^{-1} in the potential range between 0.80 and 0.25 V (SHE) for the evaporated gold electrode (mainly oriented to the (111) plane) in the electrolyte (e) 0.1 M $HClO_4$+10^{-3} M $Cu(ClO_4)_2$+10^{-3} M KCl

chronocoulometry, obtained the changes in surface tension $\Delta\gamma$ vs electrode potential E curve for the Au (111) electrode in the electrolyte, the composition of which is almost the same as that of the electrolyte (d), and they found the maximum of $\Delta\gamma$ at 0.45 V (SHE). It should be remarkable that both Δg and $\Delta\gamma$ take the maxima at the same potential of 0.45 V (SHE); in spite of that, the potential at the maximum of Δg does not always coincide with that at the maximum of $\Delta\gamma$ as seen from Eq. 1. The derivative of Eq. 1 with E is given by

$$\partial g/\partial E = \partial\gamma/\partial E + \partial^2\gamma/\partial\varepsilon\partial E = -q_m - \partial q_m/\partial\varepsilon. \qquad (7)$$

The coincidence between the potentials at the maxima of Δg and $\Delta\gamma$, therefore, means that the term of $-\partial q_m/\partial\varepsilon$ is close to zero. In the $\Delta\gamma$ vs E curve [12, 13], the change in $\Delta\gamma$ from 0.45 to 0.25 V (SHE) was $\Delta(\Delta\gamma)$=−0.50 J m^{-2}. The difference between $\Delta(\Delta g)$=−0.80 J m^{-2} and $\Delta(\Delta\gamma)$= −0.50 J m^{-2} may result from the term associated with surface elastic strain, as surface tension cannot provide any information of surface elastic strain. There have been no studies for Cu-UPD structures on Au (111) in the electrolyte (d) or perchloric acid medium containing small amounts of sulfate (10^{-4} to 10^{-2} M). Nevertheless, the similarity in the shape of Δg vs E curve between electrolytes (b) and (d) suggests that the Cu-UPD layer in the electrolyte (d) has a honeycomb $\left(\sqrt{3}\times\sqrt{3}\right)R30°$ structure in the potential range between 0.45 and 0.30 V (SHE) and a Cu-(1×1) structure at the cathodic potential limit of 0.25 V (SHE). The structural change from the honeycomb $\left(\sqrt{3}\times\sqrt{3}\right)R30°$ to the Cu-(1×1) in the potential range between 0.45 and 0.25 V (SHE) may alter the surface elastic strain to bring the difference between $\Delta(\Delta g)$ and $\Delta(\Delta\gamma)$.

For the electrolyte (e), the CV has two cathodic peaks at 0.52 and 0.27 V (SHE) in the cathodic potential sweep and two anodic peaks at 0.53 and 0.28 V (SHE), which is consistent with the CV [19] obtained for the Au (111) electrode in 0.1 M $HClO_4$+0.01 M $Cu(ClO_4)_2$ containing 10^{-4} M Cl^- ions. In the corresponding Δg vs E curve, the maxima of Δg appear at 0.50 V (SHE) in the cathodic potential sweep and at 0.53 V (SHE) in the anodic potential sweep. The change in Δg from 0.50 to 0.25 V (SHE) in the cathodic potential sweep is $\Delta(\Delta g)$=−0.72 J m^{-2}. Shi et al. [16], using chronocoulometry, obtained the $\Delta\gamma$ vs E curve for the Au (111) electrode in 0.1 M $KClO_4$+10^{-3} M $HClO_4$+ 10^{-3} M $Cu(ClO_4)_2$+10^{-3} M KCl solution, the pH of which is higher by two than that of the electrolyte (e), although the perchlorate and chloride concentrations are the same as those of the electrolyte (e). In the $\Delta\gamma$ vs E curve [16], $\Delta\gamma$ took a maximum at 0.50 V (SHE), and the change in $\Delta\gamma$ from 0.50 to 0.25 V (SHE) was $\Delta(\Delta\gamma)$=−0.70 J m^{-2}. The coincidence between the potentials at the maxima of Δg and $\Delta\gamma$ was observed in the electrolyte (e) as well as in the electrolyte (d). In contrast to the electrolyte (d), the value of $\Delta(\Delta g)$=−0.72 J m^{-2} obtained by the present study in the electrolyte (e) deviates only slightly from that of $\Delta(\Delta\gamma)$=−0.70 J m^{-2}, which means that the surface elastic strain does not change significantly in the above potential range. The STM images [19] of Au (111) in 0.1 M $HClO_4$+ 0.01 M $Cu(ClO_4)_2$ containing 10^{-4} M Cl^- ions showed that the "(5×5)" phase was stable in the entire Cu-UPD potential range up to the onset of Cu bulk deposition. No significant potential dependence of surface strain may come from the stability of the "(5×5)" structure in the entire Cu-UPD potential range. The chronocuolometric results [15] indicated that the ratio of copper to chloride in the adlayer for the "(5×5)" structure was equal to unity. This means that the adlayer consists of a bilayer structure in which chloride is adsorbed on the copper. It has been reported that a CuCl surface layer is formed on Cu via Cu^+ in the electrolytes containing Cu^{2+} and Cl^- [39–41].

The two alternative models [19] were proposed for the "(5×5)" bilayer structure. In the first model, both the Cu as

well the Cl^- adsorbate form a "(5×5)" lattice on the Au substrate in which each Cl^- is adsorbed in a hollow site between three Cu adatoms with Cu–Cu and Cl–Cl spacings, respectively, of 0.367 nm. In contrast, in the second model, the bilayer consists of a pseudomorphic Cu (1×1) adlayer (Cu–Cu spacing, 0.288 nm) with a closed packed "(5×5)" Cl^- layer on top. In the first model, the structural arrangement and the nearest neighbor distances are very similar to that in the (111) plane of solid CuCl with a zincblende lattice, where the ions are hexagonally arranged with a distance of 0.382 nm between neighboring Cu^+ or Cl^- ions. The SEXAFS study [23] of Cu-UPD on Au (111) indicated that the copper adatoms are packed in registry with the top layer of chloride ions and supported the first model.

Factors influencing the changes in surface stress during Cu-UPD on Au(111)

Two important factors influencing the changes in surface stress of a solid metal electrode would be the changes in bond charge density of the electrode surface atoms and the atomic configuration of the surface adlayer. Ibach [42, 43] has explained the changes in surface stress in terms of the changes in bond charge density of the electrode surface atoms. It is known that a clean metal surface generates usually a tensile surface stress. According to Ibach [42, 43], on a clean metal surface, the bond charge in the missing bonds is redistributed to strengthen the backbonds, on the one hand, and to reduce the bond length between the surface atoms on the other hand, thereby generating a tensile surface stress at the surface. Moreover, the adsorption of electronegative atoms on the surface removes charge between the surface atoms and causes a compressive surface stress. In contrast, if adsorbate atoms are electron donors, the charge density between the surface bonds should be enhanced, thereby increasing the tensile stress. Electrolyte anions such as ClO_4^-, SO_4^{2-}, and Cl^- are electronegative species. Haiss et al. [44] reported that the surface stress of Au (111) in acidic electrolytes containing various anions increases to the compressive direction as the surface coverage of anions increases.

The explanation by Ibach [42, 43] may be applicable to the changes in surface stress during Cu-UPD on Au (111). In the cathodic potential sweep from 0.80 V (SHE), the desorption of electrolyte anions proceeds predominantly before the onset of Cu-UPD, thereby, the surface stress changes to the tensile direction. The adsorption of Cu atoms should cause a compressive surface stress due to the formation of Cu-Au bond. However, the surface stress still changes to the tensile direction up to the potential corresponding to the maximum of Δg, in spite of that Cu-UPD proceeds. In the potential range from the onset of Cu-UPD to the maximum of Δg, it seems that the tensile surface stress due to desorption of electrolyte anions overcomes the compressive surface stress due to adsorption of Cu atoms. It has been reported [12, 13, 16] that co-adsorption of (bi) sulfate or chloride ions with Cu atoms takes place at the potential more negative than that at the maximum of Δg. Therefore, the surface stress changes to the compressive direction. In addition to the redistribution of bond charge between surface atoms, the term of surface elastic strain associated with atomic configuration of the Cu-UPD has to be taken into consideration to explain the changes in surface stress. In sulfuric acid, a pseudomorphic Cu-(1×1) monolayer is formed on Au (111) at the cathodic limit of 0.25 V (SHE) [31, 35, 36]. As the lattice constant (a_{Cu}=0.3615 nm) of Cu is less than that (a_{Au}=0.4079 nm) of Au, the pseudomorphic Cu-(1×1) monolayer on Au (111) has the misfit of +12.8%, which would provide the changes in surface stress to the tensile direction. The molecular dynamic simulations [37] indicated that the change in surface stress to the tensile direction due to biaxial stretching of a Cu (111) slab by 12.8% is 2.78 J m^{-2}. It is known that a $\sqrt{3} \times \sqrt{7}$ adlayer is formed for adsorption of (bi) sulfate ions on Cu(111) [45] as well as Au (111) [46]. The formation of $\sqrt{3} \times \sqrt{7}$ adlayer on Cu (111) expands the top copper layer by 4% [1, 45]. The (bi) sulfate ion-induced expansion for the Cu monolayer on Au (111) reduces the misfit and the changes in surface stress to the tensile direction. Trimble et al. [37] pointed out that the changes in surface stress to the tensile direction decrease by 1.71 J m^{-2} due to co-adsorption of (bi) sulfate ions. As Trimble et al. [37] emphasized, the lattice expansion due to co-adsorption of (bi) sulfate ions would contribute to the net changes in surface stress to the compressive direction for the pseudomorphic Cu-(1×1) monolayer on Au (111) at the cathodic potential limit.

In the presence of chloride (10^{-4} M) in perchloric acid medium, the "(5×5)" structure consisting of bilayer of Cu and Cl is formed in the entire Cu-UPD potential range up to the onset of Cu bulk deposition [19]. For the "(5×5)" bilayer as supported by the SEXAFS study [20], the copper adatoms are registry with a top layer of chloride ions, and the Cu–Cu spacing is 0.367 nm, which is smaller by 4% than that (0.382 nm) for the bulk CuCl. This means that the bilayer lattice is compressed as compared to the bulk CuCl. Therefore, the formation of the "(5×5)" structure would contribute to the compressive surface stress. In perchloric acid medium, a trace amount of Cl^- ions ($\leqq 10^{-6}$ M) contained impurity, controls the CV and Cu-UPD structure. The suppression of Cu-UPD process due to perchlorate ions may result from the difference between strength of specific adsorption of perchlorate ions on Cu and Au. At present, however, there are no reliable data of the order in the strength of specific adsorption of perchlorate ions between

Cu and Au. If the specific adsorption of perchlorate ions on Au is stronger than that on Cu, the replacement of adsorbed perchlorate ions by Cu atoms on Au would need the more cathodic potential. Figure 6 shows the CV and Δg vs E curve obtained in the electrolyte (c) when the cathodic potential limit is extended to 0.10 V (SHE). It is seen from the CV in Fig. 6 that the further progress of Cu-UPD is brought by the cathodic overpotential of 0.15 V. The necessity of overpotential for the further progress of Cu-UPD suggests that the specific adsorption of perchlorate ions on Au is stronger than that on Cu. The Δg vs E curve in Fig. 6 indicated that the change in Δg from 0.40 to 0.10 V (SHE) in the cathodic potential sweep is $\Delta(\Delta g)=-0.60$ J m^{-2}. The changes in surface stress to the compressive direction in the cathodic potential sweep are enhanced with the further progress of Cu-UPD. The changes in surface stress to the compressive direction still continue up to 0.30 V (SHE) in the reverse potential sweep. Therefore, the progress of Cu-UPD in perchloric acid is very slow and may be controlled by diffusion of Cl^- ions [19].

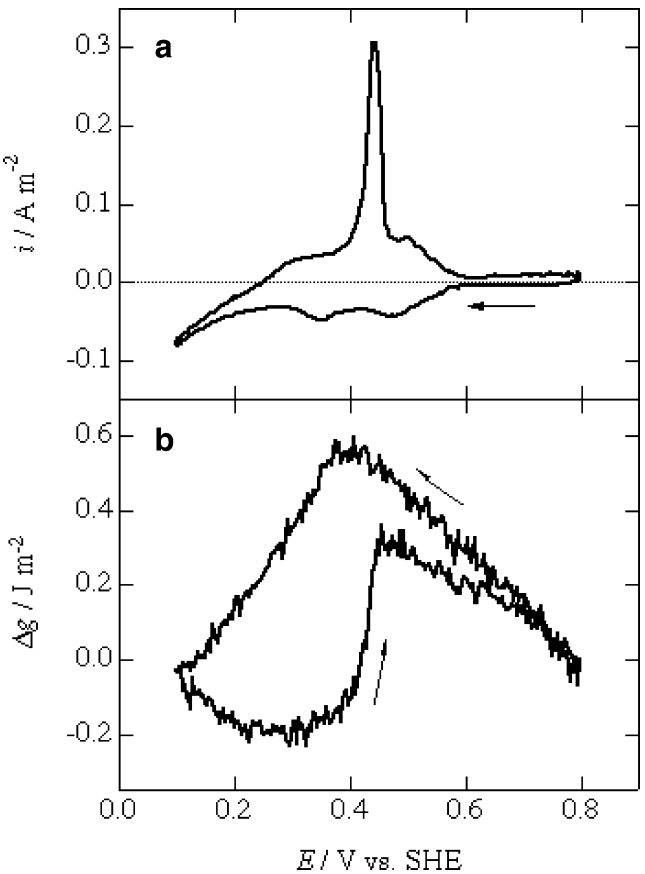

Fig. 6 **a** Cyclic voltammogram and **b** Δg vs E curve obtained at a potential sweep rate of 5 mV s^{-1} in the potential range between 0.80 and 0.10 V (SHE) for the evaporated gold electrode (mainly oriented to the (111) plane) in the electrolyte (c) 0.1 M $HClO_4$+10^{-3} M $Cu(ClO_4)_2$+10^{-3} M $KClO_4$

Conclusions

The changes in surface stress Δg of Au (111) electrode during Cu-UPD in sulfuric acid medium and perchloric acid medium with and without sulfate or chloride could be measured as a function of electrode potential E using a bending beam method. The following conclusions were drawn from the Δg vs E curves.

(1) The difference in Δg of the gold electrode between sulfuric acid media with and without Cu^{2+} was −1.1 J m^{-2} at the cathodic potential limit of 0.25 V (SHE) corresponding to the formation of pseudomorphic Cu-(1×1) monolayer.

(2) In the perchloric acid medium containing sulfate, the change in Δg from the potential of surface stress maximum to the cathodic potential limit of 0.25 V (SHE) corresponding to the complete formation of pseudomorphic Cu-(1×1) monolayer was $\Delta(\Delta g)=-0.80$ J m^{-2}, which was different from $\Delta(\Delta\gamma)=-0.50$ J m^{-2} obtained from coulometry by Shi and Lipkowski [12, 13]. The value of $\Delta(\Delta g)$ more negative than that of $\Delta(\Delta\gamma)$ was ascribed to the change of surface elastic strain due to the structural change of Cu-UPD layer from the honeycomb $(\sqrt{3}\times\sqrt{3})R30°$ to the Cu-(1×1).

(3) In the perchloric acid medium containing chloride, the change in Δg from the potential of surface stress maximum to the cathodic potential limit of 0.25 V (SHE) was $\Delta(\Delta g)=-0.72$ J m^{-2}, which was close to $\Delta(\Delta\gamma)=-0.70$ J m^{-2} obtained from coulometry by Shi et al. [16]. The value of $\Delta(\Delta g)$ close to that of $\Delta(\Delta\gamma)$ suggested that the surface strain was independent of potential due to the stability of the "(5×5)" Cu–Cl bilayer observed in the entire Cu-UPD potential range. In the perchloric acid medium without sulfate and chloride, the small change in surface stress up to the cathodic potential limit of 0.25 V (SHE) indicated that perchlorate ions suppressed the progress of Cu-UPD. The cathodic overpotential of 0.15 V was needed for further progress of Cu-UPD with large change in surface stress of $\Delta g=-0.60$ J m^{-2} to the compressive direction, suggesting that the specific adsorption of perchlorate ions on Au is stronger than that on Cu.

(4) The change in bond charge density of the electrode surface atoms and the atomic configuration of the surface adlayer were listed as two important factors influencing the change in surface stress during Cu-UPD. The formation of Cu-Au bond and co-adsorption of electronegative species such as (bi) sulfate or chloride ions with copper atoms remove charge between the surface atoms and cause a compressive surface stress. In sulfuric acid medium or perchloric

acid medium containing sulfate, pseudomorphic Cu-(1×1) monolayer on Au (111) provides the change in surface stress to the tensile direction due to the misfit of 12.8%, whereas adsorption of (bi) sulfate ions on the Cu-(1×1) monolayer induces the lattice expansion by 4% and reduces the tensile surface stress. In perchloric acid medium containing chloride, the "(5×5)" bilayer is formed in which the copper adatoms are registry with a top layer of chloride ions, and the Cu-Cu spacing is smaller by 4% than that for the bulk CuCl, thereby contributing to the compressive surface stress.

References

1. Herrero E, Buller LJ, Abruna HD (2001) Chem Rev 101:1897
2. Shuttleworth R (1950) Proc R Soc Lond A 63:444
3. Lipkowski J, Schmickler W, Kolb DM, Parsons R (1998) J Electroanal Chem 452:193
4. Láng GG, Heusler KE (1994) J Electroanal Chem 377:1
5. Láng GG, Heusler KE (1999) J Electroanal Chem 472:168
6. Gutman EM (1995) J Phys Condens Matter 7:L663
7. Ueno K, Seo M (1999) J Electrochem Soc 146:1496
8. Seo M, Serizawa Y (2003) J Electrochem Soc 150:E472
9. Friesen C, Dimitrov N, Cammarata RC, Sieradzki K (2001) Langmuir 17:807
10. Toney MF, Gordon JG, Samant, Borges GL, Melroy OW (1992) Phys Rev B 45:9362
11. Seo M, Yamazaki M (2004) J Electrochem Soc 151:E276
12. Shi Z, Lipkowski J (1994) J Electroanal Chem 364:289
13. Shi Z, Lipkowski J (1994) J Electroanal Chem 365:303
14. Shi Z, Lipkowski J, Gamboa M, Zelenay P, Wieckowski A (1994) J Electroanal Chem 366:317
15. Shi Z, Wu S, Lipkowski J (1995) Electrochim Acta 40:9
16. Shi Z, Wu S, Lipkowski J (1995) J Electroanal Chem 384:171
17. Magnussen OM, Hotlos J, Nichols RJ, Kolb DM, Behm RJ (1990) Phys Rev Lett 64:2929
18. Hachiya T, Honbo H, Itaya K (1991) J Electroanal Chem 315:275
19. Hotlos J, Magnussen OM, Behm RJ (1995) Surf Sci 335:129
20. Toney MF, Howard JN, Richer J, Borges GL, Gordon JG II, Melroy OR (1995) Phys Rev Lett 75:4472
21. Melroy OR, Borges GL, Blum L, Abruna HD, Albarelli MJ, Samant MG, McMillan M, White JH, Gordon JG II (1988) Langmuir 4:728
22. Tadjeddine A, Tourillon G, Guay D (1991) Electrochim Acta 36:1859
23. Wu S, Lipkowski J, Tyliszczak T, Hitchcock AP (1995) Prog Surf Sci 50:227
24. Trimble TM, Cammarata RC, Sieradzaki K (2003) Surf Sci 531:8
25. Stoney GG (1909) Proc R Soc Lond A 32:172
26. Láng GG, Seo M (2000) J Electroanal Chem 490:98
27. Láng GG, Ueno K, Ujvári M, Seo M (2000) J Phys Chem B 104:2785
28. Láng GG, Seo M, Heusler KE (2005) J Solid State Electrochem 9:347
29. Rokob EA, Láng GG (2005) Electrochim Acta 51:93
30. Batina N, Will T, Kolb DM (1992) Faraday Discuss 94:93
31. Green MP, Hanson KP (1992) J Vac Sci Technol A 10:3012
32. Tadjeddine A, Lahrichi A, Tourillon G (1993) J Electroanal Chem 360:261
33. Borges GL, Kanazawa KK, Gordon JGII, Ashley K, Richer J (1993) J Electroanal Chem 364:281
34. Watanabe M, Uchida H, Miura M, Ikeda N (1994) J Electroanal Chem 384:191
35. Manne S, Hansma PK, Massie J, Elings VB, Gewirth AA (1991) Science 251:183
36. Ikemiya N, Miyaoka S, Hara S (1994) Surf Sci 311:L641
37. Trimble T, Tang L, Vasilljevic N, Dimitrov, van Schilfgaarde M, Friesen C, Thompson CV, Seel SC, Floro JA, Sieradzki K (2005) Phys Rev Lett 95:166106
38. Kongstein OE, Bertocci U, Stafford GR (2005) J Electrochem Soc 152:C116
39. Láng GG, Ujvári M, Horányi G (2002) J Electroanal Chem 522:179
40. Doblhofer K, Wasle S, Soares DM, Weil KG, Weinberg G, Ertl G (2003) Z Phys Chem 217:479
41. Doblhofer K, Wasle S, Soares DM, Weil KG, Ertl G (2003) J Electrochem Soc 150:C657
42. Ibach H (1994) J Vac Sci Technol A 12:2240
43. Ibach H (1997) Surf Sci Rep 29:193
44. Haiss W, Nichols RJ, Sass JK, Charle KP (1998) J Electroanal Chem 452:199
45. Wilms M, Broekmann P, Stuhlmann C, Wendelt K (1988) Surf Sci 416:121
46. Gregory JE, Gao X, Weaver MJ (1994) J Electroanal Chem 375:357